

Macroscopic quantum tunneling in PdO nanoparticles

Francisco Ascencio C. Reyes-Damián
Roberto Escudero

Instituto de Investigaciones en Materiales, Universidad Nacional Autónoma de México
Mexico City, 04510 Mexico
fascencioag@gmail.com

March 23, 2021

Abstract

We studied the physical behavior of PdO nanoparticles at low temperatures, which presents an unusual behavior clearly related to macroscopic quantum tunneling. The samples show a tetragonal single phase with P42/mmc space group. Most importantly, the particle size was estimated at about 5.07 ± 1.97 nm. Appropriate techniques were used to determine the characteristic of these nanoparticles. The most important aspect of this study is the magnetic characterization performed at low temperatures. It shows a peak at 50 K in zero field cooling mode (ZFC) that corresponds to the Blocking temperature (T_B). These measurements in ZFC and field cooling (FC) indicate that the peak behavior is due to different relaxation times of the asymmetrical barriers when the electron changes from a metastable state to another. Below T_B in FC mode, the magnetization decreases with temperature until 36 K; this temperature is the crossover temperature T_{Cr} , related to the anisotropy of the barriers, indicative of macroscopic quantum tunneling.

1 Introduction

The study of the magnetic properties of materials has been a topic of great interest in nanoparticles because of the unusual new properties. For instance, molecular magnets offer interesting characteristics useful to different systems. In general, compounds formed by nanostructures could be one of the most simple manners to observe the effects of macroscopic quantum tunneling, MQT.

One relevant characteristic seen in ferromagnetic materials is that their magnetic characteristics change when the size is reduced to a limit; this is the critical value. In this limit, the magnetic behavior changes to superparamagnetism, SP. At that point, the thermal assisted SP can be blocked by random thermal fluctuations due to spin orientations and could be frozen as the temperature decreases. At low temperatures, the thermal fluctuations are frozen and consequently become trapped and can not surpass the magnetic barriers of metastable states. At this point, quantum tunneling magnetic effects, MQT takes place because nanoparticles show a dramatic increase in the surfaced to volume ratio; the effect occurs because of anisotropy of the barriers. At this point, MQT clearly is observed, and also other characteristics as spin glass, behavior, paramagnetic, and or superparamagnetism characteristics.

Experimentally some of those features related to the MQT can be seen at low temperatures: the blocking and crossover temperatures. Both features are quite dependent and related to the anisotropy

of the arising energy barriers in the metastable states that allow the spin transference between two states.

The characteristics and properties observed in nanomaterials are intrinsic properties of electronic interaction between them. In 3d and 4d series atoms, band structure changes dramatically, changing the surface because of the narrowing of the bands and distances. One aspect that is important in the study of the cumulous of nanoparticles. Accordingly, to carry out and understand this behavior is quite important to know the coordination of the structures formed by the cumulous.

Pd samples with macroscopic dimensions behave quite differently as nanosize scale; this behavior was observed by many authors [1, 2, 3, 4].

When nonmagnetic material is in the critical size [5, 6] studies performed in Metal-Oxygen compounds show that the magnetic behavior is strongly related to oxygen vacancies, substitutional and interstitial defects, as well as surface defects of the nanomaterials.[7, 8, 9] However, one of the most unusual magnetic characteristics in nanomaterials is the observation of properties that can be related to macroscopic quantum tunneling of the magnetization (QTMs or MQT) [10, 11, 12, 13, 14, 15, 16, 17, 18]. The MQT has been observed mainly in nanoparticles compounds of metal oxides; the two important characteristics or features can be observed at low temperatures, they are the blocking T_B and the cross-over temperatures, T_{Cr} . [19, 20, 21, 22, 23]

It is important to mention that the study of metallic oxides is attractive because of numerous applications that can be used in different fields; i.e. catalysis, as precursors to the synthesis of superconductors, electronic devices, biomedical applications, and gas sensors [24, 25, 26, 27, 28]. Additionally these studies become relevants when the compounds are low-dimensional materials as in thin films, wires, or nanoparticles. Nowadays, it is well known that size, shape, and surface structure, and physicochemical properties as in optical, electronics, and magnetism behaves differently than in bulk. Related to this study, Palladium Oxide, PdO, nanoparticles have attracted attention because of the uniques physicochemical properties. PdO in bulk is a nonmagnetic compound [29]. It presents a tetragonal symmetry, Cooperite, in which Pd atoms occupy D_{2h} and O atoms occupy D_{2d} positions [30]. In the structure, the Pd atoms are coordinated by 4 oxygen atoms in a planar manner, while O atoms are coordinated with 4 Pd atoms, forming a tetrahedron. PdO is a P-type semiconductor, with a direct gap. In previous studies by many authors has been observed that the bandgap is close to 2 eV [31, 32] which has industrial interest mainly because its photocatalytic characteristics [33] used in the oxidation of CH_4 [34], and in sensors [35]. Actually, some methods have been used to synthesize PdO nanostructures; as sol-gel[36],thermo-hydrolyzation assisted by microwave [37]. Related to this work the synthesize was performed using a simple method that a continuation will be described.

2 Experimental Details

PdO nanoparticles were synthesized by an alkali salt method, synthesized with concentrations of 0.125 g of $Pd(NO_3)_2 \cdot 2 H_2O$ (Sigma Aldrich, 99 %), 0.125 g of Li_2CO_3 (Ripley Scientific) and 2.5 g of NaCl (Sigma Aldrich) were mixed in an agate mortar and milled for 30 minutes until obtain a fine powder. Samples were heated at 400 °C in a furnace at atmospheric pressure. Finally, the obtained samples were washed five times with distilled water in order to eliminate residues of the reaction.

2.1 Characterization

Characterized of the samples were carried out by X-ray diffraction (XRD) performed with a Bruker (D8 Advance) and Cu-K $_{\alpha}$ radiation, determined from 2Θ range of 20° – 120°. The phase was identified using the Crystallographic Open Database (COD) and crystalline structure refined with Rietveld method using the BGMN program [38] and the graphical interface Profex. Peak profiles were modeled to determine the crystal size using the Debye-Scherrer formula [39]. Transmission

electron microscopy (TEM), JEOL JEM-2010F FasTem microscope operated at 200 kV. The samples for TEM were prepared, depositing a drop of the solution into the mesh Cu grid. The Raman spectra were recorded in a Thermo Scientific confocal microscope equipped with micro-Raman using three different excitation sources: 532 nm (2.33 eV), 633 nm (1.95 eV), and 780nm (1.58 eV); measurements were carried out in the 50–3000 cm^{-1} range. Optical properties were characterized by UV–visible spectroscopy with a Thermo Evolution 220 spectrophotometer. Finally, magnetization as a function of temperature ($M(T)$) and magnetization as a function of the magnetic field ($M(H)$) were determined using a Quantum Design magnetometer (MPMS).

3 Results and Discussion

3.1 X-Ray Diffraction

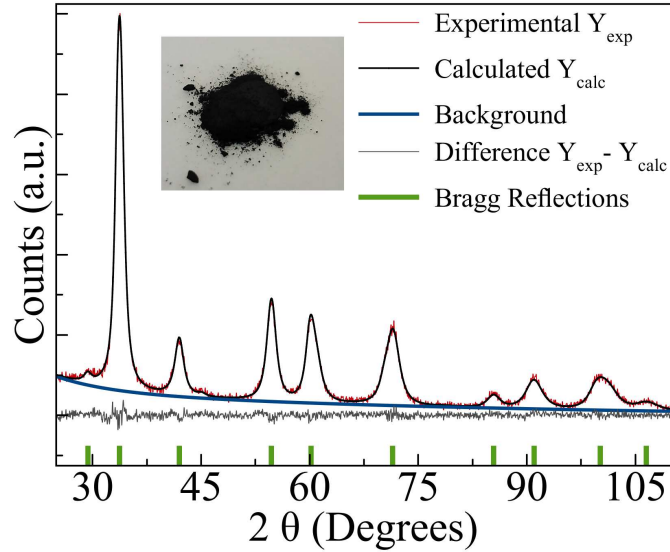


Figure 1: X-ray diffraction pattern measured with $\text{CuK}\alpha$ radiation and bragg reflections of reference 96–100–9032 taken from the Crystallographic Open Database. The right inset shows the Rietveld refinement of PdO nanoparticles diffraction pattern. The bottom line is the difference between experimental and calculated pattern. A photograph of the powder sample is also shown in the left inset.

The crystallographic structure of the PdO nanoparticles was determined by X-ray diffraction (XRD). XRD pattern is shown in the figure 1, there we show the XDR measurements of PdO (nano)powders in which the PdO tetragonal phase was detected. The right inset of the figure 1 shows the Rietveld refinement of the sample; the red line is the experimental data, in the inset, the black line is the calculated pattern. At the bottom of the diagram, the differences between the experimental and calculated points are shown in gray color. Vertical blue marks at the bottom are displayed and correspond to the Bragg positions for the phase. Finally, the background was modeled with a Lagrangian polynomial. From Rietveld refinement, we see the phase identified and

modeled with tetragonal PdO phase according to the Crystallographic Open Database (COD) number 96 – 100 – 9032 described by the space group P42/mmc. The average crystal size was 10.31 ± 0.83 nm. Cell parameters were calculated the resulting lattice parameters were $a = 0.3042 \pm 0.0001$ and $c = 0.5356 \pm 0.0003$ nm, according to the space group # 131. Finally, Rietveld residues were: $R_{wp} = 6.91\%$, $R_{exp} = 6.51\%$ and $R_{wp}/R_{exp} = 1.06$.

3.2 Transmission Electron Microscopy

Transmission electron microscopy was carried out to obtain structural and morphological information of the samples. In the figure 2 (a), HRTEM micrograph is presented. It is observed that the nanoparticles have an irregular polyhedron shape. The first particle of around 5 nm presents the interplanar distances $d_1 = 2.195 \text{ \AA}$ and $d_2 = 2.523 \text{ \AA}$, with an angle between planes of $\theta = 52.07^\circ$. These reflections correspond to the (1 1 0) and (0 1 1) planes oriented along the $[-1\ 1\ -1]$ axis zone from the FFT lattice fringes are resolved. Figure 2 (b) shows another nanoparticle with 4 nm of diameter with the FFT, is seen only the plane (0 1 1). In the figure 2 (c), the nanoparticles average diameter were 5.07 ± 1.97 nm. measured using a total of 200 particles. The structure of these nanoparticles was confirmed through electron diffraction, figure 2 (d), the pattern was matched with the PdO crystal structure. The reflections were indexed as the (0 1 0), (0 1 1), (0 1 2), (1 1 2), and (0 1 3) crystallographic planes, according to COD, # 96 – 100 – 9032. The optical and magnetic properties of palladium oxide nanoparticles are related to grain boundaries or defects in the nanoparticle structure; hence, the HRTEM images permit a clear observation of their fine features. With TEM studies, it can be observed that the produced nanoparticles are single crystals without the presence of twins or grain boundaries.

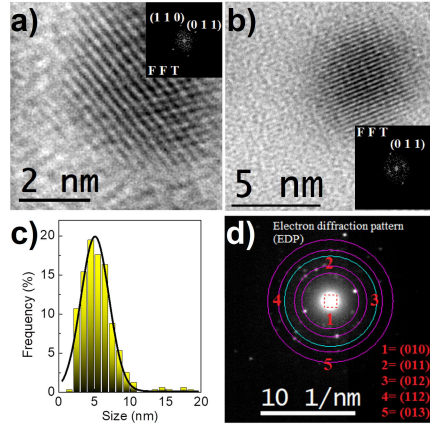


Figure 2: (a) HRTEM image of a very small PdO nanoparticles with the corresponding FFT, (b) another HRTEM image for a representative nanoparticle with the corresponding FFT, (c) the nanoparticles size distribution (d) electron diffraction pattern.

3.3 Raman and UV-visible Spectroscopy

Raman spectra were collected at room temperature from the sample powders to obtain detailed structural information related to normal vibrational modes of the samples with three wavelengths $\lambda =$

532, 633, and 780 nm or excitation energies of 2.33, 1.95, and 1.59 eV, in order to observe resonance phenomena.

Assuming that the PdO compound has a tetragonal symmetry with space group $P42/mmc$ (#131) and point group $D4h$, and according to the factor group analysis, this compound will display two vibrational Raman active modes (B_{1g} and E_g). The remaining normal modes of vibration are located in the IR region (A_{2u} , $2E_u$) and a silence mode B_{2u} [40, 32].

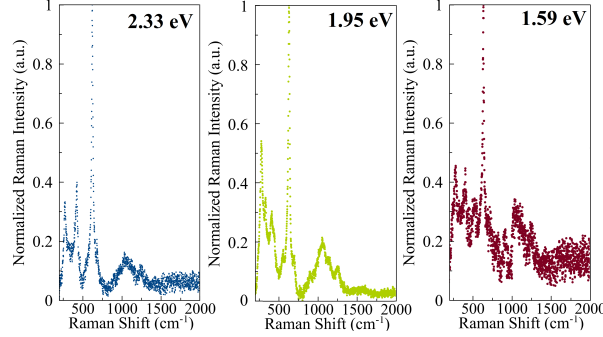


Figure 3: Full Raman spectra of PdO nanoparticles at room temperature for three excitation energies 2.33, 1.95 and 1.59 eV

In the figure 3, the normalized Raman spectra of the samples measured at room temperature with three different wavelengths (excitation energy) are shown. It is observed that the spectra show some Raman peaks below 1500 cm^{-1} , in Table 1 a list of the peaks are presented for the three excitation energies.

A careful analysis of the Raman spectra (Figure 4) for each energy shows that the PdO nanoparticles have three main peaks related to B_{1g} between the frequencies: $[620.62\text{--}630.83]\text{ cm}^{-1}$, peaks between the frequencies $[425.09\text{--}401.66]\text{ cm}^{-1}$ which corresponds to E_g and finally the vibrational mode between $[273.01\text{--}278.24]\text{ cm}^{-1}$ correspond to X_8 mode [36]. Besides many other peaks related to second order processes overtones, prohibited modes and combinations of normal modes were observed [41]. It is clear in the figure 4 that when the sample was measured with the wavelength of 633 nm (1.95 eV) the peaks were better defined and new peaks appeared at different frequencies which could be the resonance effects. No peaks related to vibrations of compounds containing carbon were detected. The absence of those peaks is indicative of the purity of the samples.

The optical properties of the single crystal particles of PdO were measured. Figure 5 (a) shows the optical absorption spectra of the sample perform at room temperature. In this spectrum, we observe a strong absorption intensity in the near UV and violet region. From this measurement, the optical band gap was estimated from the absorbance spectrum using the Tauc-plot method [42, 43, 44]. Considering a direct transition, the bandgap value was determined to be 1.90 eV as presented in the figure 5 (b). The estimated bandgap values are in agreement with values proposed by [45] for PdO thin films, also in theoretical studies by DFT, close values have been obtained [46]. In different studies of PdO, some values have been found, which are in the range of $[0.8\text{--}2.67]\text{ eV}$. The discrepancy of the values could be related to the structural defects at the surface, such as oxygen vacancies and confinement effects related to particle size reduction.

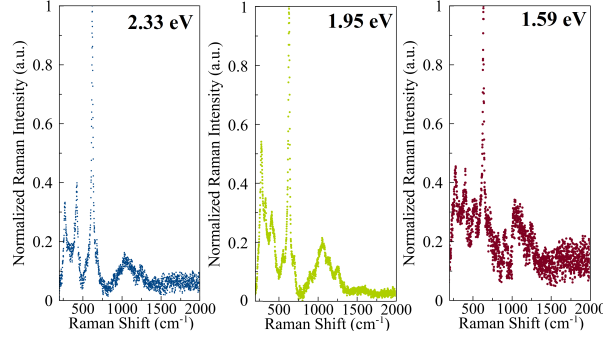


Figure 4: Comparison of Raman spectra of PdO nanoparticles around the main peak for different excitation energy

Table 1: Raman peaks obtained from Fig. 3.

2.33 eV	1.95 eV	1.59 eV
273.01	277.73	278.24
425.09	331.93	401.66
620.62	409.36	519.3
680.02	552.02	630.83
1062.13	628.80	661.04
1257.21	695.28	911.74
	1057.43	
	1142.61	
	1254.29	

3.4 Magnetism

The magnetization $M(T)$ as function of temperature for PdO nanoparticles was determined with an applied magnetic field of 1000 Oe in two modes of magnetization, as usual; zero field cooling (ZFC) and field cooling (FC) modes as can be seen in the figure 6. The difference between ZFC and FC curves indicates a large anisotropic field.

In addition we performed measurements of the inverse magnetization versus temperature which gives additional information about the behavior shown figure 7. A clear paramagnetic behavior is seen from room temperature to about 100 K. Below this temperature an incipient ferromagnetism arises. The para-ferromagnetic transition has been observed in other nanoparticles and the transition was associated with oxygen vacancies [47]. At low temperature the Curie Weiss temperature (θ_{C-W}) behavior is very small, fitting gives values between -1.9 K or to about 4.5 K. However, additional structure at around 50 K, is seen in figure 6. This characteristic we related to the metastable states when the nanoparticles are transported from one metastable state to the other, depending of the applied magnetic field. We related this characteristic or behavior with a macroscopic quantum

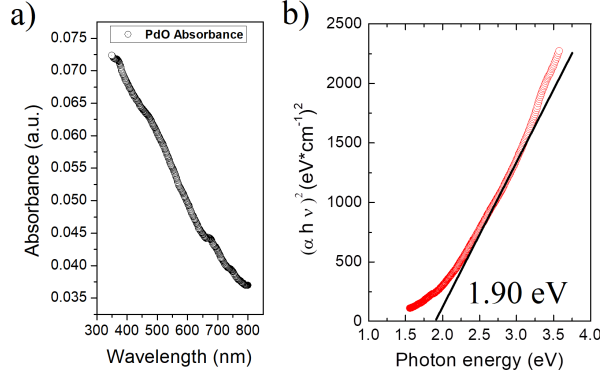


Figure 5: (a) Optical absorption of the PdO nanoparticles, (b) Tauc plot for direct transition. The bandgap was estimated as 1.9 eV

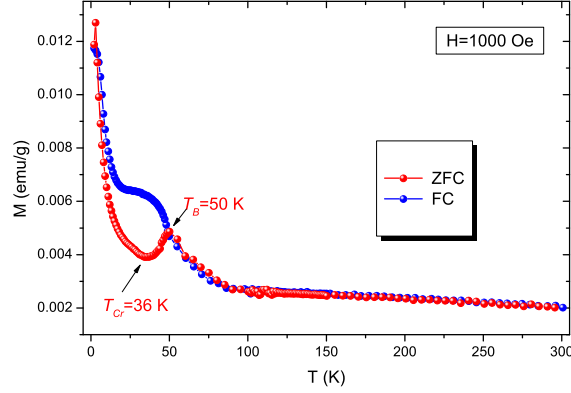


Figure 6: Magnetization of PdO nanoparticles as function of temperature measured at 1000 Oe in ZFC and FC modes. The arrows marks the blocking temperature (T_B) and the crossover temperature (T_{Cr})

tunneling [48, 49]. Two features give information of the magnetization; the blocking temperature T_B [50] and the crossover temperature, T_{Cr} . The Fig. 6 shows those characteristics temperatures at 50 K and 36 K respectively. Knowing $T_B = 36$ K and the mean volume of the nanoparticles ($V = 6.541 \times 10^{-20} \text{ cm}^3$). The magnetic anisotropy constant (K) can be calculated by the the formula 1 [51], were k_B is the Boltzman constant.

$$K = 25k_B T_B V^{-1} \quad (1)$$

The value for K is $1.891 \times 10^6 \text{ erg/cm}^3$ is not comparable with bulk PdO because this last is not magnetic.

Below T_B the magnetization decrease with the temperature until 36 K, this temperature is the crossover temperature and separate the thermally activated regime T_{Cr} from the quantum tunneling

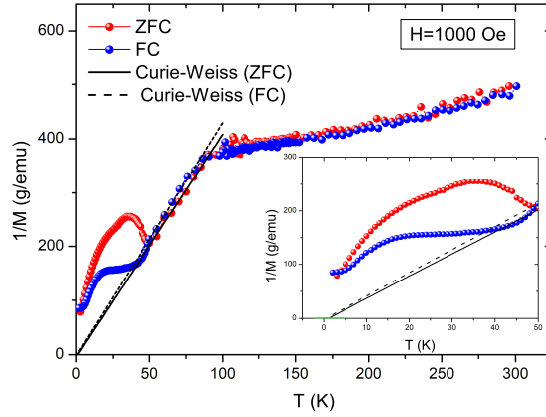


Figure 7: A paramagnetic behavior was determined in the temperature range 100 - 300 of temperature with the inverse of M as function of temperature. For temperatures between 50-100 Curie-Weiss fits gives a small θ_{C-W} . Inset show the low temperature-depend of $1/M$ in order to appreciate the range of values for θ_{C-W}

regime [13]. Below $T_{Cr} = 36$ K, MQT effects take place and one can re-observed superparamagnetic state even when the thermal energy is smaller than the magnetic energy barrier [23, 48].

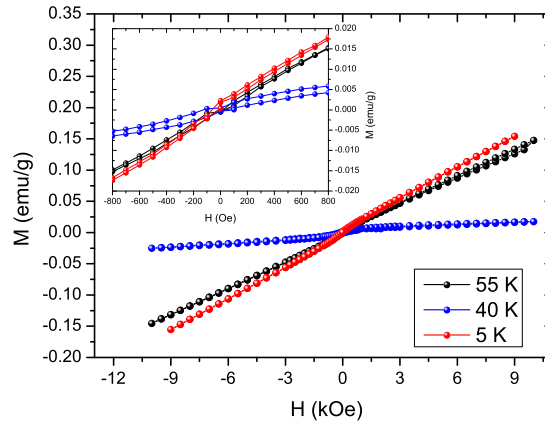


Figure 8: Magnetization of PdO nanoparticles as function of H at different temperatures. Inset shows the low field-dependent magnetization of the nanoparticles. Hysteresis loop shows small hysteresis at 40 K in the blocked state

The magnetization of the nanoparticles was measure as a function of magnetic field H in order to confirm the superparamagnetism state below T_{Cr} and above T_B . The field-dependent of magnetization was measured using three different temperatures, see figure 8. At the lowest temperature,

5 K, there is no hysteresis, and the large magnetization values are related to superparamagnetic characteristics. This magnetic behavior corresponds with the expected characteristic in a quantum tunneling regime ($T < T_{Crossover}$). The value of the magnetization in the blocked state (40K) is less than the value of the magnetization measured at 5 K. Measurements present small hysteresis and a remanent magnetization $M_r=6.57 \times 10^{-4}$ emu/g with non symmetric coercive field $H_{C+}=82$ Oe and $H_{C-}=-128$ Oe related with the possible coexistence antiferromagnetic state. Above the blocking temperature, 55 K, the behavior is superparamagnet, and the hysteresis is negligible. We assume that superparamagnetism is due to the small size of the particle (~ 5 nm).

4 Conclusions

In summary, this work presented a magnetic study of PdO nanoparticles in which we observed macroscopic quantum tunneling phenomena due to very small nanoparticles. The particle size was estimated at about 5.07 ± 1.97 nm from the TEM measurements. The Samples were analyzed by transmission electron microscopy in which the irregular shapes of the nanoparticles were observed. Using UV-VIS and Raman spectroscopy, the sample was analyzed spectroscopically. For the Raman studies, three excitation energies were used: 2.33, 1.95, and 1.59 eV ($\lambda= 532, 633$ and 780 nm), and observed the main peaks of PdO, besides the resonance phenomena, were observed. The UV-VIS measurements were performed, the behavior shows a strong absorption near to UV region. The bandgap value was estimated as 1.90 eV using Tauc-plot method. Finally, the most important aspect of this study is that we found a process related to macroscopic quantum tunneling of magnetization at low temperatures.

5 acknowledgements

Thanks to M.Sc. A. Bobadilla for the He supply. To R. Hernandez for the technical assistance in TEM. To A. Pompa and A. Lopez for technical support. We acknowledge DGAPA-PAPIIT Grant No. IT101920, F. Ascencio thanks to the DGAPA-UNAM, for the support through the Postdoctoral Scholarship

References

- [1] Y. Oba, T. Sato, T. Shinohara, Physical Review B **78**(22), 224417 (2008)
- [2] T. Shinohara, T. Sato, T. Taniyama, Physical Review Letters **91**(19), 197201 (2003)
- [3] C. Xiao, H. Ding, C. Shen, T. Yang, C. Hui, H.J. Gao, The Journal of Physical Chemistry C **113**(31), 13466 (2009)
- [4] Y.T. Jeon, G.H. Lee, Journal of Applied Physics **103**(9), 094313 (2008)
- [5] A. Cox, J. Louderback, S. Apsel, L. Bloomfield, Physical Review B **49**(17), 12295 (1994)
- [6] G.L. Nealon, B. Donnio, R. Greget, J.P. Kappler, E. Terazzi, J.L. Gallani, Nanoscale **4**(17), 5244 (2012)
- [7] D. Gao, J. Zhang, J. Zhu, J. Qi, Z. Zhang, W. Sui, H. Shi, D. Xue, Nanoscale Research Letters **5**(4), 769 (2010)
- [8] K. Punia, G. Lal, S.K. Barbar, S.N. Dolia, P.A. Alvi, S. Dalela, S. Kumar, Vacuum **184**, 109921 (2021)
- [9] B. Choudhury, A. Choudhury, Journal of Applied Physics **114**(20), 203906 (2013)

- [10] E.M. Chudnovsky, L. Gunther, Physical review letters **60**(8), 661 (1988)
- [11] E.M. Chudnovsky, Journal of applied physics **73**(10), 6697 (1993)
- [12] B. Barbara, W. Wernsdorfer, L. Sampaio, J. Park, C. Paulsen, M. Novak, R. Ferré, D. Mailly, R. Sessoli, A. Caneschi, et al., Journal of magnetism and magnetic materials **140**, 1825 (1995)
- [13] X. Zhang, J. Hernandez, J. Tejada, R. Ziolo, Physical Review B **54**(6), 4101 (1996)
- [14] R. Kodama, Journal of magnetism and magnetic materials **200**(1-3), 359 (1999)
- [15] L. Thomas, B. Barbara, Journal of low temperature physics **113**(5), 1055 (1998)
- [16] B. Barbara, L. Gunther, Physics World **12**(3), 35 (1999)
- [17] W. Wernsdorfer, E.B. Orozco, B. Barbara, A. Benoit, D. Mailly, N. Demoncy, H. Pascard, O. Kubo, H. Nakano, IEEE transactions on magnetics **34**(4), 973 (1998)
- [18] B. Barbara, W. Wernsdorfer, Current Opinion in Solid State and Materials Science **2**(2), 220 (1997)
- [19] X. Zhang, J. Tejada, Journal of Applied Physics **75**(10), 5637 (1994)
- [20] R. Kodama, C. Seaman, A. Berkowitz, M. Maple, Journal of Applied Physics **75**(10), 5639 (1994)
- [21] X. Zhang, R. Ziolo, E. Kroll, X. Bohigas, J. Tejada, Journal of magnetism and magnetic materials **140**, 1853 (1995)
- [22] M. Ibrahim, S. Darwish, M. Seehra, Physical Review B **51**(5), 2955 (1995)
- [23] C. Xiao, J. Zhang, J. Xu, W. Tong, B. Cao, K. Li, B. Pan, H. Su, Y. Xie, Scientific reports **2**(1), 1 (2012)
- [24] J.C. Védrine, ChemSusChem **12**(3), 577 (2019)
- [25] R.J. Cava, Journal of the American Ceramic Society **83**(1), 5 (2000)
- [26] M. Greiner, M. Helander, Z. Wang, W.M. Tang, J. Qiu, Z. Lu, Applied Physics Letters **96**(21), 103 (2010)
- [27] M.A. Shahbazi, L. Faghfour, M.P. Ferreira, P. Figueiredo, H. Maleki, F. Sefat, J. Hirvonen, H.A. Santos, Chemical Society Reviews **49**(4), 1253 (2020)
- [28] D. Nunes, A. Pimentel, A. Gonçalves, S. Pereira, R. Branquinho, P. Barquinha, E. Fortunato, R. Martins, Semiconductor Science and Technology **34**(4), 043001 (2019)
- [29] R. Ahuja, S. Auluck, B. Johansson, M. Khan, Physical Review B **50**(4), 2128 (1994)
- [30] K. Hass, A. Carlsson, Physical Review B **46**(7), 4246 (1992)
- [31] T. Kumari, R. Gopal, A. Goyal, J. Joshi, Journal of Inorganic and Organometallic Polymers and Materials **29**(2), 316 (2019)
- [32] R. Bardhan, H.F. Zarick, A. Schwartzberg, C.L. Pint, The Journal of Physical Chemistry C **117**(41), 21558 (2013)
- [33] S. Veziroglu, J. Hwang, J. Drewes, I. Barg, J. Shondo, T. Strunskus, O. Polonskyi, F. Faupel, O. Aktas, Materials Today Chemistry **16**, 100251 (2020)
- [34] J.G. McCarty, Catalysis Today **26**(3-4), 283 (1995)
- [35] A. Das, D.H. Ko, C.H. Chen, L.B. Chang, C.S. Lai, F.C. Chu, L. Chow, R.M. Lin, Sensors and Actuators B: Chemical **205**, 199 (2014)
- [36] Q. Zhao, H. Li, L. Zhang, Y. Cao, Journal of Photochemistry and Photobiology A: Chemistry **384**, 112032 (2019)

- [37] Z. Li, J. Song, D.C. Lee, A. Abdelhafiz, Z. Xiao, Z. Hou, S. Liao, B. DeGlee, M. Liu, J. Zeng, et al., *Electrochimica Acta* **329**, 135166 (2020)
- [38] J. Bergmann, P. Friedel, R. Kleeberg, (1998)
- [39] H.P. Klug, L.E. Alexander, *X-ray diffraction procedures: for polycrystalline and amorphous materials* (1974)
- [40] J. Remillard, W. Weber, J. McBride, R. Soltis, *Journal of applied physics* **71**(9), 4515 (1992)
- [41] J. McBride, K. Hass, W. Weber, *Physical Review B* **44**(10), 5016 (1991)
- [42] W. Li, *Materials chemistry and physics* **99**(1), 174 (2006)
- [43] N. Kumar, S.S. Parui, S. Limbu, D.K. Mahato, N. Tiwari, R.N. Chauhan, *Materials Today: Proceedings* (2020)
- [44] F. Ascencio, J. Estevez, L. Rangel-Gamboa, L. Bazán-Díaz, R. Mendoza-Cruz, R. Herrera-Becerra, *Materials Today Communications* **25**, 101614 (2020)
- [45] C.J. Huang, F.M. Pan, H.Y. Chen, Li-Chang, *Journal of Applied Physics* **108**(5), 053105 (2010)
- [46] M.K. Bruska, I. Czekaj, B. Delley, J. Mantzaras, A. Wokaun, *Physical Chemistry Chemical Physics* **13**(35), 15947 (2011)
- [47] B. Sarkar, A. Bandyopadhyay, J. Mandal, A. Deb, P. Chakrabarti, *Journal of Alloys and Compounds* **656**, 339 (2016)
- [48] Y. Xu, B. Yao, Q. Cui, *RSC advances* **6**(9), 7521 (2016)
- [49] J. Tejada, R. Ziolo, X. Zhang, *Chemistry of materials* **8**(8), 1784 (1996)
- [50] I. Bruvera, P. Mendoza Zélis, M. Pilar Calatayud, G.F. Goya, F.H. Sánchez, *Journal of Applied Physics* **118**(18), 184304 (2015)
- [51] X.H. Li, C.L. Xu, X.H. Han, L. Qiao, T. Wang, F.S. Li, *Nanoscale research letters* **5**(6), 1039 (2010)